Geometry Effects on Steady and Acoustically Forced Shear-Coaxial Jet Sprays

S. Teshome[*+], I.A. Leyva[+&], J. Rodriguez[+], D. Talley[+]
[*]UCLA, Los Angeles, CA, USA, [+]Air Force Research Lab, Edwards, CA, USA
steshome@ucla.edu and ivett.leyva@edwards.af.mil

Abstract

The mixing process on four shear-coaxial injectors with different outer-to-inner jet area ratios and varying inner jet post thickness was examined experimentally. The experiments were conducted at ~1.5MPa with varying outer-to-inner jet momentum flux ratios ($J \sim 2 - 20$), with and without a pressure antinode perturbation at the jet exit. Nitrogen was used as the test fluid. High speed back-lighting movies, acoustic pressure measurements and temperature exit profiles were the main diagnostics used. Proper orthogonal decomposition was applied to the intensity fluctuation of the high-speed images to extract spatial and temporal characteristics of the dominant flow structures. The extent of the influence of outer-to-inner momentum flux ratio on mixing was dependent on the injector geometry. The inner jet lengths for large outer-to-inner area ratio injectors were more influenced by increasing momentum flux ratios. The response of the injector flows to a pressure antinode was also dependent on the particular geometry. One injector showed a strong response to acoustics regardless of J, while the response of the other two injectors to a pressure antinode was dependent on J.

Introduction

Coaxial injectors have proven to be one of the most effective and simple means of delivering propellants in combustion devices such as in liquid rocket engines (LREs). Their application in LREs in the United States spans from the development of the J-2 engine to the space shuttle main engine. Since injector flows are directly involved in processes that take place inside combustors, it is crucial to understand how they contribute to, as well as how they are affected by, unsteady physical mechanisms that could lead to rough combustion or even combustion instabilities. A fundamental understanding of the interactions between injector flows and chamber combustion can be aided by first isolating the fluid dynamic aspects from the reactive flow processes, and studying the coupling of non-reactive injector flow instabilities with external pressure perturbations.

Shear-coaxial flows consist of a circular core or inner jet and an annular or outer jet. In the near field region, where the potential cores of both the inner and outer jets exist, two shear-layers develop: an inner one between the inner and outer jet, and an outer one between the outer jet and the ambient fluid[1]. The development of instabilities in the individual shear layers and their interactions have a direct impact on the eventual instability characteristics of the entire flow field. Several studies[2-4] investigate the existence and behavior of vortex structures in the near-field region of single-phase coaxial jets with similar and different densities. It is shown that for outer to inner jet velocity ratios exceeding unity ($R = U_o/U_i > 1$), coherent structures in the outer shear layer dominate those in the inner shear layer. The influence of these coherent structures on the overall dynamics of the flow field calls for an understanding of the factors leading to their formation. Detailed studies on the development and growth of natural instabilities in a single circular jet[6] or a single circular jet with coflow[7] reveal two of the most significant natural modes of instability: the axisymmetric and the first azimuthal or helical modes. These modes have comparable amplification rates over most of the core region downstream of the exit, with the helical mode eventually dominating the flow field farther downstream. It is shown[1] that the development of the outer shear layer of a coaxial jet behaves as the shear layer of a single jet, while the development of the inner shear layer behaves as that of a single jet issuing into an external coflow.

In LRE applications understanding the mixing between the inner jet, usually the oxidizer, and the outer jet, usually the fuel, is of paramount importance for a successful design. Since the growth and development of the shear layers is integral to the mixing of the two jets, one way of quantifying the degree of mixing is to determine the inner jet potential core length.[1, 8-10] The inner jet potential core ends once the inner shear layer converges on the jet axis. The current study relies on back-lit high speed movies to measure inner jet dark-core lengths, which are related to the potential core.[13, 15]

This study continues the experiments performed in the same facility[11-15] examining the behavior of shear-coaxial nitrogen (N_2) jets with and without the presence of a transverse acoustic field. It examines the baseline flow of four injectors with different inner jet post thickness to diameter ratios, different outer to inner jet area ratios, and a range of momentum flux ratios. The flow response to a pressure antinode forcing condition, where the coaxial jet is exposed to the maximum local pressure fluctuations in a transverse acoustic field is also examined. Dark-core length measurements are made to determine the effect of momentum flux ratio and of acoustic forcing on mixing. Proper orthogonal decomposition (POD) analysis is also used to extract spatial and temporal

[&]Corresponding author: ivett.leyva@edwards.af.mil

dominant flow structures in the inner shear layer of the baseline and acoustically forced flows. The goal is to gain a better understanding of the evolution of flow instabilities and underline the critical differences in the flow stability characteristics of different geometries.

Experimental Set-up and Computational Methods

The experiments were carried out at the Air Force Research Laboratory in Edwards, CA. Figure 1 shows a schematic of the experimental facility. The inner and outer jets as well as the chamber pressurization flow were supplied by ambient temperature, high pressure N_2 lines (critical pressure is 3.4 MPa, and critical temperature is 126.2 K). Counter-flow heat exchangers using liquid nitrogen were used to independently cool the inner and outer jets. An unshielded Omega type-E thermocouple with a bead diameter of 0.25mm, mounted on top of a 3D array of linear positioning stages, was used to measure the radial temperature profile of the coaxial jet within one inner jet diameter from the exit plane. Porter mass flow meters (123-DKASVDAA) were used to measure the inner and outer jet flow rates, which were controlled via metering valves. The jets issued into the test section (Fig. 1) of the inner chamber halfway between the two piezo-sirens located at opposite ends of the chamber. Each piezo-siren was fitted with a waveguide that transitioned from a circular to a rectangular cross-section. The inner chamber was used to maximize the amplitude of acoustic oscillations generated by the piezo-sirens. However, both the inner and main chambers were maintained at the same static pressure, which was measured with a Stellar ST1500 pressure transducer.

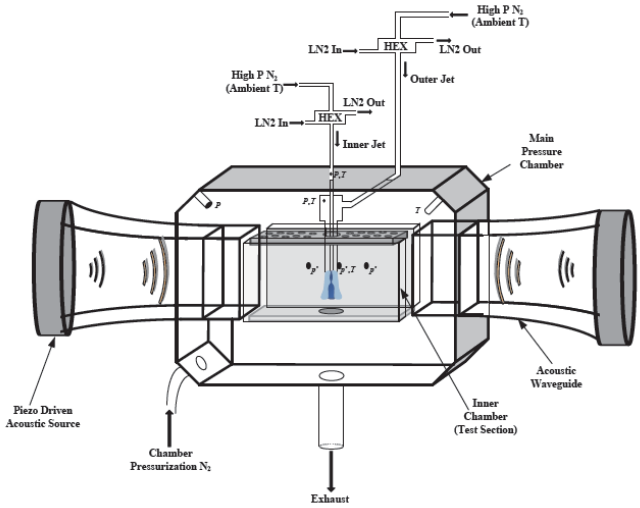

Figure 1 Schematic of experimental chamber and fluid systems

The outer to inner jet momentum flux ratio ($J = \rho_o U_o^2 / \rho_i U_i^2$), velocity ratio ($R$), and other flow conditions were determined based on thermophysical properties evaluated at the measured chamber pressure, and jet exit temperatures. Kulite absolute (CCQ-093) and differential (XCQ-093, XCE-093) pressure transducers were used for making high-speed acoustic pressure measurements. These pressure transducers were placed along the inner chamber wall, where one transducer was located directly behind the jet, and two others inside the injector plenums. The acoustic wave signals were generated using a Fluke 292 arbitrary waveform generator. A Trek PZD2000A high-voltage amplifier fed a continuous sine wave from the waveform generator to each piezo-siren. The resulting acoustic waves from each piezo-siren were traveling waves that propagated transversely along the waveguide. Using signals that were in-phase (0^o phase difference), a pressure antinode (PAN) condition was

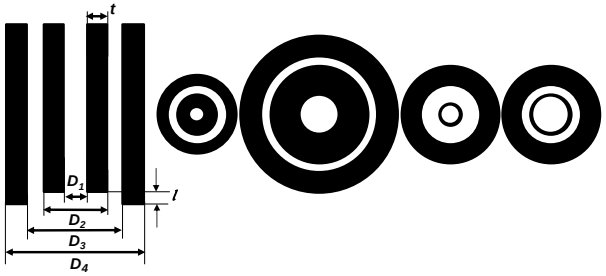

Figure 2. Injector schematics

Injector	D1 mm	D2 mm	D3 mm	D4 mm	t/D1	Ao/ Ai	l/D1
LAR-thick	0.51	1.59	2.42	3.18	1.05	12.9	0
SAR-thick	1.47	3.96	4.70	6.35	0.84	2.9	-0.1
LAR-thin	0.70	0.89	2.44	3.94	0.13	10.6	0.2
SAR-thin	1.40	1.65	2.44	3.94	0.09	1.6	0,-0.5

Table 1. Summary of injector dimensions

created in the center between the two piezo-sirens where the injector was situated, with maximum pressure perturbation.

Figure 2 shows a schematic of the injector's exit plane view. Table 1 provides a summary of the injector exit dimensions. A negative value of l means the inner jet is recessed. As seen from the table, two injectors have large outer-to-inner jet cross-sectional area ratio (LAR), and two have small area ratios (SAR). Two injectors have small inner jet lip thickness to inner jet diameter ratios (thin) and two have large ratios (thick).

As mentioned above, one of the main parameters used to assess the effect of J and acoustic forcing on coaxial jet mixing is the "dark-core length" of the inner jet measured from high-speed back-lit images. A xenon arc lamp was used to provide a back-lit image of the coaxial jet, which is visualized using a Phantom v7.1 CMOS camera at framing rates exceeding 20 kHz. For a detailed discussion of how the dark-core length is defined and measured see [13]. Briefly, the original images (Fig. 3a) are first converted, or thresholded, to a black and white image using the MATLAB subroutine "im2bw" (Fig. 3b). The threshold level is determined using the MATLAB subroutine "graythresh". This subroutine uses Otsu's method[16] and it is based on the zeroth and first cumulative moments of the gray-level histogram. Once a black and white image is obtained, the length of the jet is determined by drawing a contour around the black and white image and measuring the axial length of the longest contour attached to the injector (Fig. 3c).

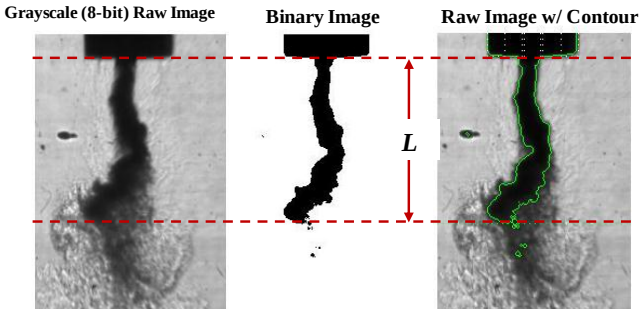

Figure 3. Measurement of dark-core length: (a) original image (b) black and white image after thresholding (c) Contour used to determine axial length (L)

Proper orthogonal decomposition (POD) of the high-speed images has proven to be a powerful means for extracting relevant qualitative and quantitative information from an otherwise complicated and noisy set of images. A pixel intensity data matrix, **B** for a set of images may be represented [17-19] as

$$\mathbf{B} = \sum_{k=1}^{M} a_k(t)\phi_k(x) \tag{1}$$

where a_k are vectors of temporal amplitude coefficients, ϕ_k are vectors of proper orthogonal modes, k is the mode number, and M is the number of modes. The decomposition was achieved by first arranging all the pixel intensity values of all frames into a single data array, whereby the pixel intensities from one frame occupied one row of the data array. Thus, a set of N consecutive frames, each with an n×m pixel resolution, constituted an N by $n \times m$ data array. The temporal mean of the data array was subtracted in order to eliminate the DC component of the intensity values resulting in a matrix $\widetilde{\mathbf{B}}$ of intensity fluctuations. The method of singular value decomposition was implemented in MATLAB using a built-in subroutine to represent the matrix of intensity fluctuations as

$$\widetilde{\mathbf{B}} = \mathbf{Q}\mathbf{V}^{\mathrm{T}} \tag{2}$$

where **Q** is an N by N matrix composed of column vectors a_k, and **V** is an N by $n \times m$ matrix composed of column vectors ϕ_k from Eq. (1). The matrix **Q** is the product of an orthogonal matrix of left singular vectors and a diagonal matrix of singular values of $\widetilde{\mathbf{B}}$. The different modes were arranged in decreasing order of significance as dictated by the magnitude of the singular values of the decomposition. In order to identify the existence of conjugate mode pairs[18], which have a temporal phase difference of $\pm 90^{o}$ and also have similar ϕ_k, the cross-power spectral density of their amplitude coefficients, a_k and b_k was computed as

$$\mathrm{CPSD} = \sum_{s=0}^{N-1} \mathrm{corr}(a_k, b_k) e^{-iws} \tag{3}$$

where corr(a_k, b_k) represents the cross-correlation of a_k and b_k.

Results and Discussion

The experiments described here were performed under subcritical (reduced pressure, P_r = 0.44) pressure conditions with the inner jet in liquid phase and the outer jet in gas phase at temperatures well above the saturation temperature of N_2. The flow conditions are summarized in Table 2. The behavior of the inner jet dark-core length for baseline conditions without acoustic excitation is shown in Figure 4 for the four geometries studied.

As previously noted, for coaxial jets of different densities, the outer to inner jet momentum flux ratio, *J*, is one of the governing parameters of coaxial jet mixing and thus it is chosen as the x-axis. In the present work, for a set of test conditions, the outer-to-inner jet density ratio ($S = \rho_o/\rho_i$) was held approximately constant while R was varied. Thus, the variation in *J* in these studies resulted mainly due the variation in *R*. The recess of the inner tube with respect to the outer tube is given in Table 1. The inner jet tube for the LAR-thin injector stuck out by about $0.2D_1$ to allow for visual confirmation that the inner jet injector tube was not oscillating due to the outer jet flow.

Note that there were negligible differences in L_B/D_1 between the flushed and recessed configurations of the SAR-thin injector. Also note that this specific geometry showed the least amount of effect from *J*. In fact, L_B/D_1 remains almost flat for the range of *J* studied. Moreover, for low *J* flows, the SAR-thick and SAR-thin injectors showed comparable L_B/D_1, which were significantly lower than that of the LAR-thin and LAR-thick injectors. This was in agreement with previous observations[5,19] that show the potential core is longer for larger area ratios. The large difference in L_B/D_1 between the LAR-thin and LAR-thick injectors may be attributed to the presence of the recirculation zone behind the thick inner tube post of the LAR-thick injector that entrained a significant portion of the inner jet fluid for *J* = 2 and higher. For large *J*, the data for all injectors appeared to asymptote to the same L_B/D_1. However, due to experimental limitations, large enough *J* were not attainable to verify this trend.

Next, the behavior of three geometries for a low and high *J* value will be examined for baseline conditions and when subjected to a pressure antinode (Fig. 5). The values of *J* chosen span about an order of magnitude and are good descriptors of what happens at low *J* values, when flows are usually more receptive to acoustic disturbances, and at high *J* values when such receptivity subsides. For all injectors, the forcing frequencies were within 5-10% of the fundamental resonance frequency of the outer jet injector tube. Since the back-lit images reveal best the dense inner jet, the discussion will be limited to the dark-core flow region and the identifiable flow structures on its periphery.

For the SAR thin injector, baseline, at *J* = 2.1, the inner jet breaks into droplets and forms a spray within the field of view. Periodic surface instability flow structures can be seen on the periphery of the inner jet. The dominant modes depicted by the light and dark lobes in the proper orthogonal mode (POM) image show what appear to be symmetric flow structures close to the injector exit, but transitioned to antisymmetric structures further downstream. The CPSD magnitude spectra show that the peak frequencies were unaffected by increasing *J*. This may be explained by how soon the inner and outer jets attained a single jet behavior, thereby rendering the effect of the coflow nonexistent. The baseline case for *J* = 17 shows a slightly shorter dark core length, which is surprising since for the other geometries studied, the relative size difference in the dark core length was larger over a similar range of *J*. Note the large difference on the POM images between the two cases. For the large *J* case, the modes are clearly antisymmetric from the start but their inception is farther downstream from the injector exit plane. The spread angle and the wavelength of the disturbances appear to be larger than for the low *J* case.

When subjected to a PAN condition, the lower *J* value case shows strong symmetric disturbances that annihilate the inner jet flow. For the higher *J* value, although symmetric disturbances were not as strong, they nevertheless were still prevalent as evident in the POM images and the spectra. As a matter of fact, the spectra showed strong response to external forcing regardless of the *J* value. This was also evident by the lack of any remnants of the low-frequency peaks present in the baseline spectra. The baseline spectrum is superimposed to the forced spectrum (dashed line) for all three geometries so that a direct comparison can be made.

For the LAR-thin injector, *J* = 2, the dark-core region broke up into a fine droplet spray within the field of view. The presence of a larger shear force at the jets' interface than for lower *J* values also aided in the formation of a fine mist of droplets on the periphery of the inner jet flow. The dominant flow structures were antisymmetric, their inception being about $1\text{-}2D_1$. The CPSD magnitude spectral peak was relatively broad centered around 2 kHz. Under a PAN condition, a varicose mode is discernible in the image, with the growth of the resulting symmetric structures relatively subdued.

The higher shear present in the *J* = 21 case aided in the break-up and dispersion of the inner jet resulting in rapid mixing with the outer jet at closer distances to the injector exit. Accordingly the dark-core length became shorter. The inception point of the antisymmetric structures seen with POD was closer to the injector exit and the broad peak in the magnitude spectrum shifted to higher frequencies. The flows under PAN forcing were virtually similar to the corresponding baseline flows. Although the flow disturbance in the inner jet was considerably reduced compared to the lower *J* case, its presence was still evident in the images.

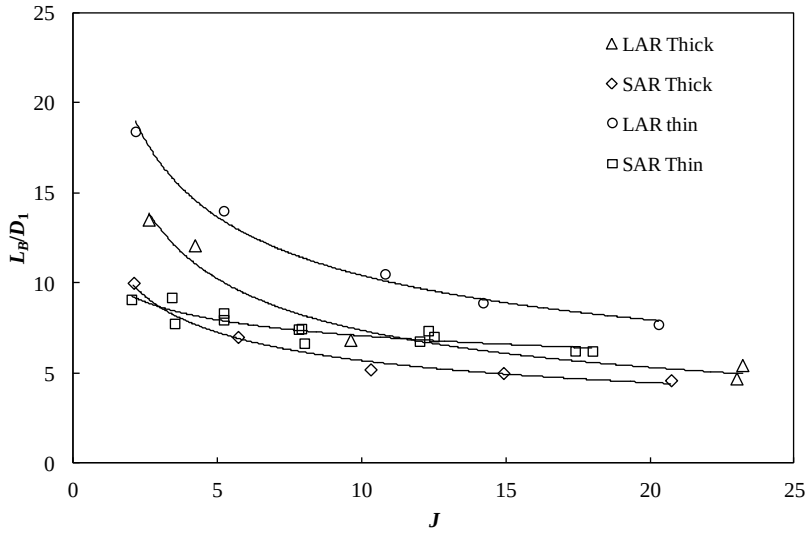

Figure 4. Summary of normalized dark-core lengths for different geometries at baseline conditions

In contrast to the LAR-thin and SAR-thin injector flows, the SAR-thick inner injector post created a larger recirculation zone just below the thick post and surrounding the inner jet flow. For J = 2.1, the entrainment by the outer flow caused most of the recirculation zone to be filled with the lower momentum inner jet fluid. The presence of the dense, dark fluid in the recirculation zone created a perception of "necking" in the dark-core flow. Further downstream, the dark-core could no longer maintain its coherence and was fully dispersed into droplets. The POM image shows distinct antisymmetric structures denoting the presence of helical disturbances, and the CPSD magnitude shows a low frequency peak. For PAN conditions the fluid inside the recirculation zone mainly consisted of the lower momentum inner jet fluid, and the sense of rotation was such that a counterflow existed at the inside boundary of the outer jet. Thus, for J = 2.1 and higher, the outer shear-layer vortices had the same sense of rotation as the fluid in the recirculation zone, unlike for lower J flows. One would then expect that coupling between these flow regions during varicose disturbances due to the PAN forcing may induce symmetric flow structures on the inner jet surface. However, as Figure 5 shows, besides imparting a merely irregular and dispersive flow pattern, the PAN forcing did not result in a periodic, varicose type of disturbance pattern on the inner jet.

For the case J = 21, the recirculation zone was completely filled with the inner jet fluid. The remaining inner jet fluid underwent increased dispersion resulting in a shorter dark-core. Together with the recirculation flow, the inner jet started to form a conical dark-core region. The dark-core length was reduced by about 50% compared with the lower J case. The POM also shows antisymmetric structures. However, unlike the LAR-thin flows, the peaks in the magnitude spectra stayed at low frequencies. Under PAN forcing, the higher J value case exhibited symmetric flow disturbances. They appeared to start just beyond the end of the recirculation zone, rolled-up and entrained the inner jet fluid further downstream.

Injector	J	R	T_{ch} K	ρ_{ch} kg/m^3	P_{ch} MPa	T_o K	$\dot{m}_o$ mg/s	ρ_o kg/m^3	U_o m/s	Re_o $x10^4$	T_i K	$\dot{m}_i$ mg/s	ρ_i kg/m^3	U_i m/s	Re_i $x10^4$
SAR-thin	2.0	6.9	246	21	1.49	195	450	27	6.6	1.1	109	925	630	0.96	1.5
SAR-thin	17	20	217	24	1.48	194	1300	27	19	3.1	108	925	638	0.95	1.4
LAR-thin	2.1	7.4	220	23	1.50	205	2212	25	22	6.3	107	725	646	2.9	2.1
LAR-thin	20	22	220	23	1.50	204	4633	26	45	13	110	482	622	2.0	1.6
SAR-thick	2.1	7.3	205	25	1.50	212	1789	24	15	1.9	110	2130	622	2.0	3.3
SAR-thick	21	23	196	27	1.50	206	4385	25	35	4.7	107	1658	646	1.5	2.3

Table 2. Summary of flow conditions for figure 5

a. SAR-thin

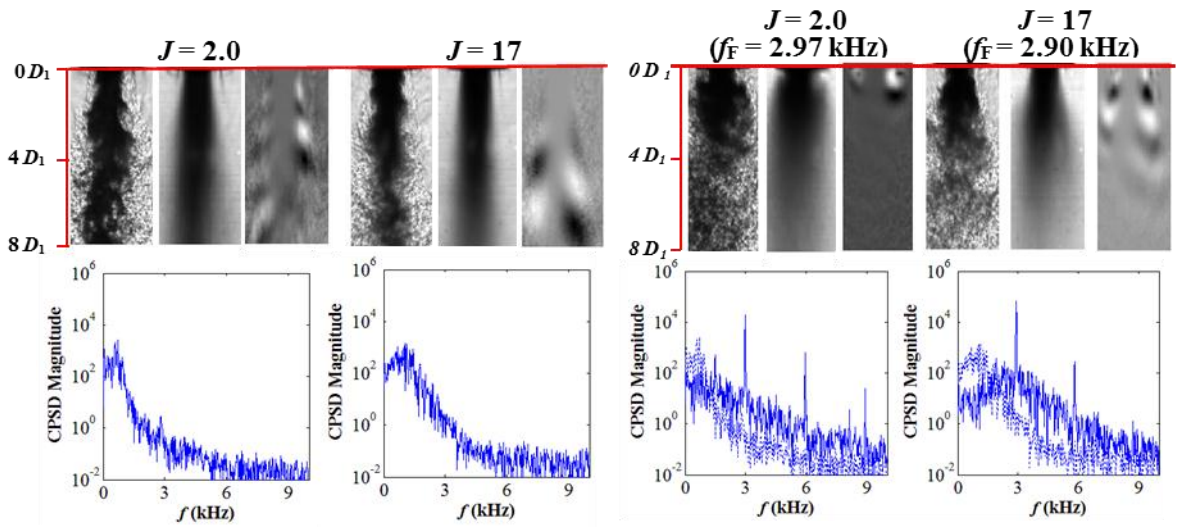

b. LAR-thin

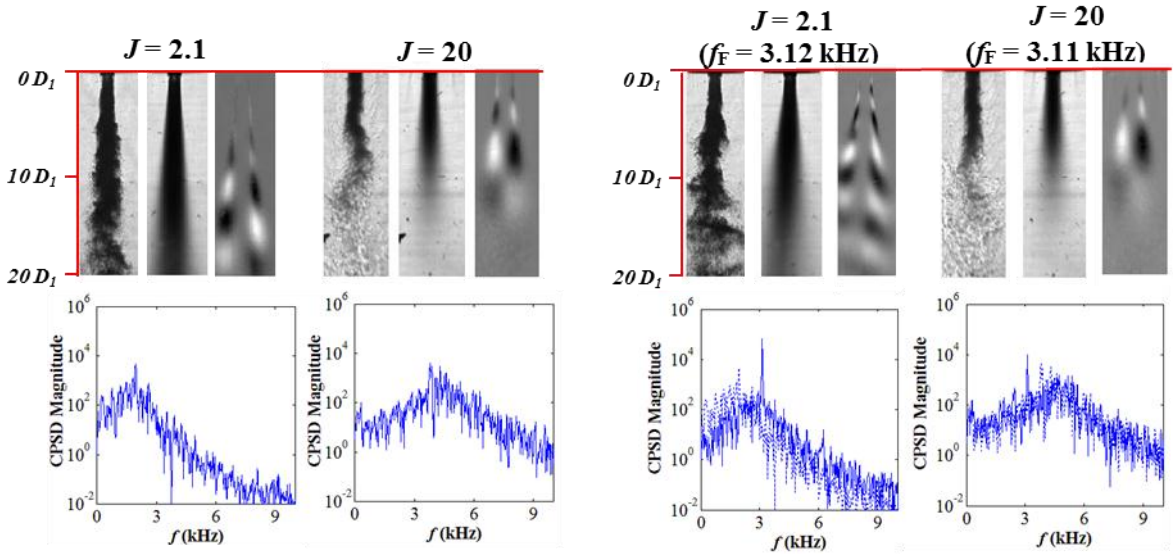

c. SAR-thick

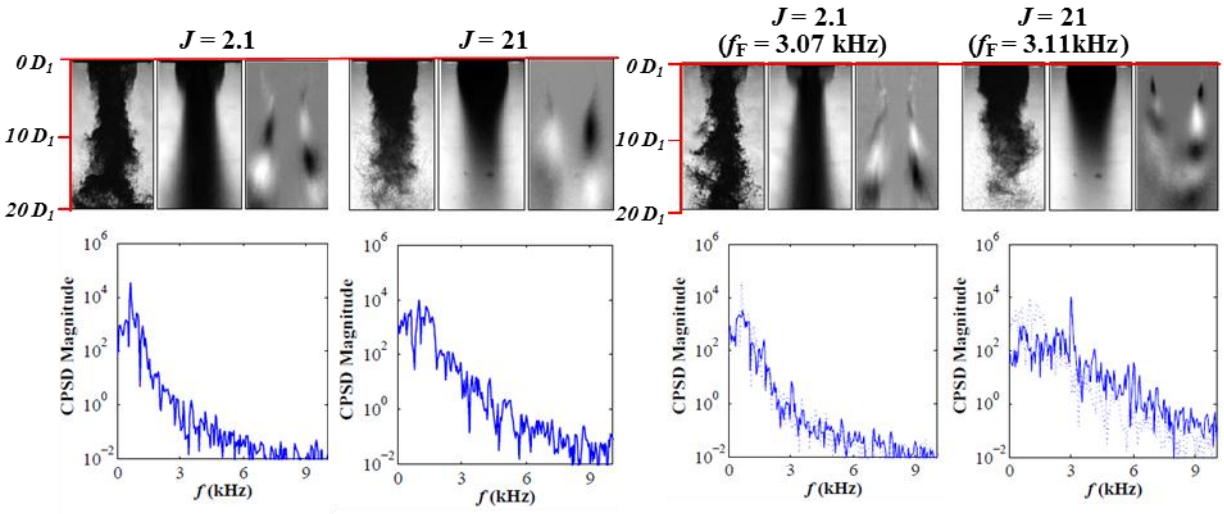

Figure 5. Baseline (left half of page) and PAN conditions (right half of page) for (a) SAR-thin (b) LAR-thin (c) SAR-thick injectors.

Summary and Conclusions

This study examined the effect of different exit geometries on the mixing characteristics as well as the behavior of flow disturbance structures with and without transverse acoustic forcing. The ratios of dark-core lengths to the inner jet diameters, which were used to assess the extent of mixing between the inner and outer jets, were reported for baseline flows using four different injector geometries. These measurements revealed that for low *J*, the small area ratio (SAR) injector flows, had significantly lower L_B/D_1 than the large area ratio flows. However, L_B/D_1 for all injectors appeared to asymptote to the same value at high enough *J*. The effect of geometry was also manifested in the response to a pressure antinode (PAN) acoustic forcing of similar *J* flows of different injector geometries. The low *J* LAR-thin injector flow showed a strong response at the PAN forcing frequency while the high *J* appeared less responsive and retained the baseline flow spectral characteristic. In contrast, the SAR-thin injector flow showed strong response at the PAN forcing regardless of *J*. The low *J* SAR-thick injector flow showed no response at the forcing frequency, while the high *J* flow did. Thus, these key traits shed some light on the significance of how simple design alterations in injector geometries may bring about drastic changes in the mixing and response of shear-coaxial jet flows to external pressure disturbances.

Acknowledgements

The authors would like to thank Mr. Randy Harvey for his invaluable contributions in running and maintaining the experimental facility. This work is sponsored by AFOSR under Dr. Mitat Birkan, program manager.

References

[1] Ko, N. W. M. and Kwan, S. H., *J. Fluid Mech.* 73: 305-332 (1976)
[2] Dahm, W. J. A., Frieler, C.E., and Tryggvason, G. *J. Fluid Mech*. 241:371-402 (1992)
[3] Wicker, R.B. and Eaton, J.K.., *AIAA Journal* 32:542-546 (1994)
[4] Balarac, G., Mtais, O. and Lesieur, M. *Phys. Fluids* 19, 075102 (2007).
[5] Gladnick, P. G., Enotiadis, A. C., LaRue, J. C. and Samuelsen, G. S., *AIAA Journal* 28: 1405-1414 (1990)
[6] Cohen, J. and Wygnanski, L., *J. Fluid Mech*. 176: 191-219 (1987)
[7] Michalke, A. and Hermann, G., *J. Fluid Mech.* 114: 343-359 (1982)
[8] Mayer, W. and Krülle, G., *J. Propulsion and Power* 11: 3 (1995)
[9] Villermaux, E., Rehab, H. and Hopfinger, E.J., *Meccanica* 29: 393-401 (1994)
[10] Rehab, H., Villermaux, E. and Hopfinger, E.J., *J. Fluid Mech*. 345:357-381 (1997)
[11] Davis, D.W., *Ph.D. Thesis*, Penn State University (2005)
[12] Davis, D.W. and Chehroudi, B., J. *Propulsion and Power* 23: 2 (2007)
[13] Leyva, I.A., Chehroudi, B. and Talley, D., *AIAA 2007-5456*
[14] Leyva, I.A., Rodriguez, J.I., Chehroudi, B. and Talley, D., *AIAA 2008-950*
[15] Rodriguez, J. I., *Ph.D. Thesis*, University of California Los Angeles (2009)
[16] Otsu, N., *IEEE transactions on Sytems, Man, and Cybernetics* 9:62-66 (1979)
[17] Chatterjee, A., *Current Science* 78: 7 (2000)
[18] Arienti, M, and Soteriou M.C., *Phys. Fluids* 21:112104 (2009)
[19] Champagne, F.H., and Wygnanski, I.J. *Int. J. Heat Mass Transfer* 14: 1445-1464 (1971)